Journal of Alloys and Compounds 510 (2012) 87–91

Contents lists available at SciVerse ScienceDirect

Journal of Alloys and Compounds

journal homepage: www.elsevier.com/locate/jallcom

Influence of MnO_2 on the sintering behavior and magnetic properties of $NiFe_2O_4$ ferrite ceramics

Jinjing Du*, Yihan Liu, Guangchun Yao, Xiuli Long, Guoyin Zu, Jia Ma

School of Materials and Metallurgy, Northeastern University, Shenyang, China

ARTICLE INFO

Article history:
Received 20 June 2011
Accepted 26 August 2011
Available online 6 September 2011

Keywords:
$NiFe_2O_4$ ferrite ceramics
Manganese dioxide (MnO_2)
Sintering behavior
Saturation magnetization
Coercivity

ABSTRACT

The samples with small amounts of MnO_2 (0, 0.5, 1.0, 1.5, 2.0, and 2.5 wt%, respectively) were prepared via ball-milling process and two-step sintering process from commercial powders (i.e. Fe_2O_3, NiO and MnO_2). Microstructural features, phase transformation, sintering behavior and magnetic properties of Mn-doped $NiFe_2O_4$ composite ceramics have been investigated by means of scanning electron microscopy (SEM), differential thermal analyzer, X-ray diffraction (XRD), thermal dilatometer and vibrating sample magnetometer (VSM) respectively. The XRD analysis and the result of differential thermal analysis indicate that the reduction of MnO_2 into Mn_2O_3 and the following reduction of Mn_2O_3 into MnO existed in sintering process. No new phases are detected in the ceramic matrix, the crystalline structure of the ceramic matrix is still $NiFe_2O_4$ spinel structure. Morphology and the detecting result of thermal dilatometer show that MnO_2 can promote the sintering process, the temperature for 1 wt% MnO_2-doped samples to reach the maximum shrinkage rate is 59 °C lower than that of un-doped samples. For 1 wt% MnO_2-doped samples, the value of the saturation magnetization (M_s) and coercivity (H_c) is 15.673 emu/g and 48.316 Oe respectively.

1. Introduction

Spinel ferrites with general chemical formulae $M^{2+}O{\bullet}M_2{}^{3+}O_3$ (where M^{2+} = Mg, Mn, Fe, Co, Cu, Zn, Ni and M^{3+} = In, Al, V, Cr, Mn, Fe) attracted many researchers because of their versatile practical applications [1,2]. Nickel-ferrite ($NiFe_2O_4$) is a cubic ferromagnetic material. It has an inverse spinel structure with Ni^{2+} ions occupying the octahedral B-sites and Fe^{3+} ions occupying both tetrahedral A-sites and octahedral B-sites. Its ferromagnetism originates from magnetic moment of anti-parallel spins between Fe^{3+} ions at tetrahedral sites and Ni^{2+} ions at octahedral sites [3–5]. The cubic inverse spinel structure provides a better chemical stability in the molten cryolite–alumina bath [6–8]. So nickel ferrite ($NiFe_2O_4$) can be used as a promising candidate for green inert anodes. It can produce environment-friendly O_2 gas during electrolysis instead of greenhouse gases [9]. Simultaneously, as a semiconductor, nickel ferrite ($NiFe_2O_4$) has attracted considerable attention in the field of technological application in a wide range of frequencies extending from microwave to radio frequency. These characteristics mentioned above are strongly dependent upon several factors such as chemical composition, method of preparation, stoichiometry, sintering time and temperature, sintering atmosphere and substitution of different ions, etc. [8].

Many efforts have been made to improve the basic properties of ferrites by substituting or adding various ions with different valence states. Generally, the substitution and dopant introduced into the nickel ferrite ($NiFe_2O_4$) matrix may result in the modification of their structural, mechanical, electrical and magnetic properties [10,11]. A minor additive in a host material also can greatly change the nature and concentration of defects, which can affect the kinetics of grain growth, grain boundary motion, pore mobility and pore removal [12]. Therefore it was the aim of this work to study the influence of MnO_2 dopant on the microstructure, promoting sintering mechanism and magnetic properties of $NiFe_2O_4$ ferrite ceramics.

2. Experimental procedure

2.1. Synthesis

Samples of $NiFe_2O_4$ composite ceramics, doped with different amounts of MnO_2 additive (i.e. x = 0, 0.5, 1.0, 1.5, 2.0, 2.5 wt%, respectively), were made from a mixture of NiO and Fe_2O_3 powder. The molar ratio of NiO to Fe_2O_3 was 1.87:1. The ceramic bodies were fabricated from high purity reagents [Fe_2O_3: 99.3% (Xincheng, China); NiO: 99.98% (Guoyao, China); MnO_2: 97.5% (Guoyao, China)]. Raw materials (NiO powder and Fe_2O_3 powder) were ground in distilled water via a ball-milling process using polypropylene jars with yttria-stabilized zirconia balls for 24 h and dried. Then the mixtures were ground with 4 vol% polyvinyl alcohol (PVA) binder and pressed at 160 MPa into blocks (70 mm × 15 mm × 8 mm) using a stainless steel die. The blocks were calcined in air at 1000 °C for 6 h to produce $NiFe_2O_4$ spinel

* Corresponding author at: School of Materials and Metallurgy, Northeastern University, 117, Box, 110004 Shenyang, China. Tel.: +86 24 83686462; fax: +86 24 83682912.
E-mail address: djzneu@yahoo.cn (J. Du).

0925-8388/$ – see front matter.
doi:10.1016/j.jallcom.2011.08.087

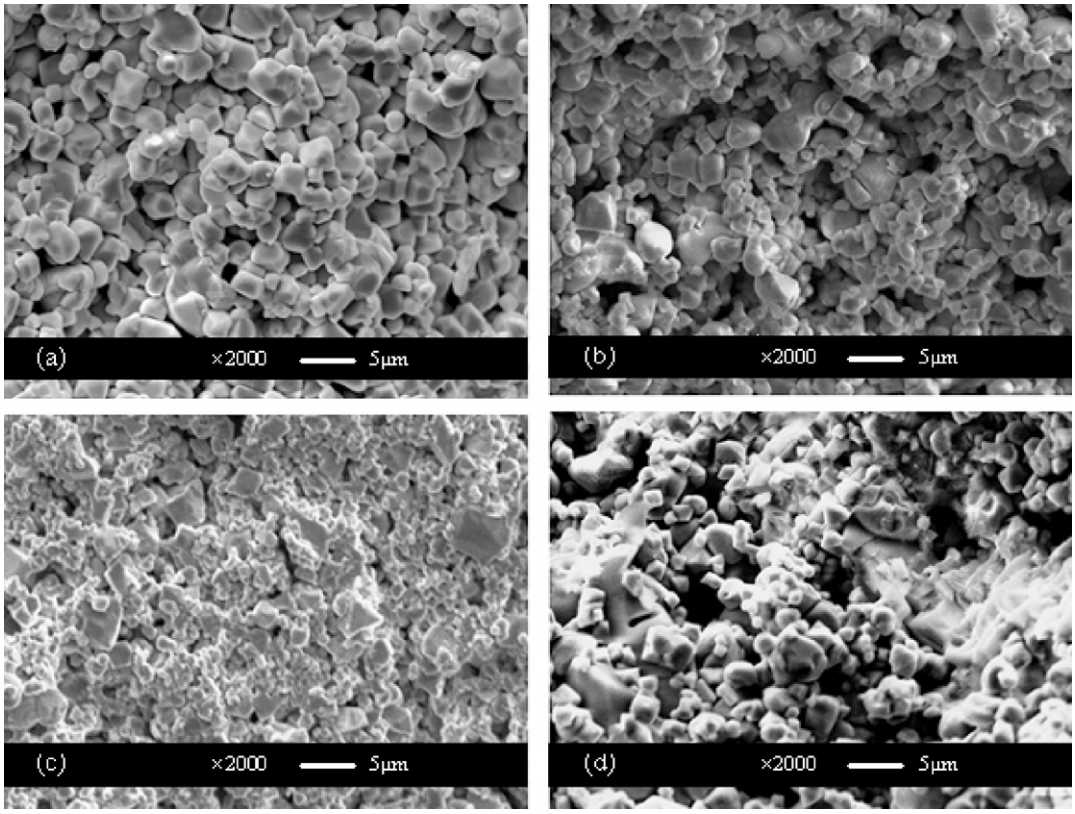

Fig. 1. SEM micrographs of the ceramic samples: (a) $x = 0$ wt% (i.e. without MnO_2 additive); (b) $x = 0.5$ wt%; (c) $x = 1.0$ wt%; (d) $x = 2.5$ wt%.

matrix material. The calcined matrix products were crushed and ball-milled with different amounts of MnO_2 for another 24 h with distilled water as dispersant, and then dried thoroughly. Adding 4 vol% PVA binders, the dried mixture was fabricated into 70 mm × 15 mm × 8 mm blocks by cold pressing at a pressure of 200 Mpa, pressure holding time 5 min.

2.2. Sintering experiment

Sintering studies for the green blocks (Φ 8.5 mm × 9.5 mm) were performed in air in a vertical dilatometer (SETSYS18 EV-24, France). The dilatometer allowed continuous monitoring of axial shrinkage. During the sintering experiment, the samples were heated at a constant rate (say, 10 K min^{-1}) to a desired temperature and then cooled down to ambient temperature.

2.3. Characterization

Fracture surface of sintered samples was characterized using scanning electron microscope (SEM) (SSX-550, Japan). The crystalline phases of the prepared samples were identified by a D/max 2RB X-ray diffractometer (Japan) with Cu Kα radiation, pip voltage 40 kV and current 100 mA.

The measurements for sintered samples of magnetic properties like saturation magnetization and coercivity were carried out in a vibrating sample magnetometer (VSM, Lakeshore 7400) at room temperature.

3. Results and discussion

3.1. Microstructure and phase identification

Selected microstructures of un-doped, 0.5, 1.0 and 2.5 wt% MnO_2-doped in air at 1200 °C for 6 h are shown in Fig. 1. As is seen in Fig. 1a, the un-doped ceramic samples have a looser structure and the grain size is about 2–4 μm. The relative density is about 90.84%. When 0.5 wt% MnO_2 was added, apparent sintering trajectories can be detected in the samples, as shown in Fig. 1b. It is also interesting to note that solid-solution phenomenon happened in 1 wt% MnO_2-doped samples. Moreover the grain size is smaller than that shown in Fig. 1a and b. And the relative density is greater than ~93.65%. However, when the content of MnO_2 is up to 2.5 wt%, the distribution of particle size is not uniform in the sintered samples, local positions are riddled with pores and the structure is not as dense as that of 1 wt% MnO_2-doped samples sintered at the same condition. It has a lower relative density ~92.61. This result suggests Mn doping can enhance the densification in comparison with un-doped samples. In the doping level ranging from 0 wt% to 1.0 wt%, Mn content has an obvious influence on the densification behavior. When the content more than 1.0 wt% (say, 2.5 wt% in this paper), it goes against the microstructure and densification. It may be attributed to the excessive Mn content, which exceeds its solubility in the $NiFe_2O_4$ ceramic matrix. This could result in that the dopant accumulates at the boundaries and increase diffusion activation energy, which is unfavorable for sintering process.

In order to identify the phases in sintered samples, a phase analysis using X-ray diffraction patterns (XRD) was performed to confirm the formation of single-phase cubic spinel ferrites and all the samples demonstrate the high crystalline structure, as shown in Fig. 2. The samples show all the characteristic peaks of ferrite material with most intense peak (3 1 1), which confirms the formation of cubic spinel structure (Fig. 1) The results obtained by XRD analysis indicate that no new phases formed in the sintered samples with the introduction of MnO_2 into ceramic matrix. It may be contributed to the entrance of Mn ions into the lattice of $NiFe_2O_4$. The calculated lattice constants for un-doped and 1 wt% MnO_2 doped samples are 8.31 Å and 8.34 Å. This increase of lattice parameter with Mn ions leads to the difference in ionic sizes of the component ions. According to the SEM micrographs in Fig. 1, it is known that the lattice distortion caused by introduction of Mn ions into the ceramic matrix is beneficial for sintering.

In addition, differential scanning calorimetry (DSC) was also applied to further analyze the phase evolution. The results from DTA curve for samples doped with 2 wt% MnO_2, as shown in Fig. 3,

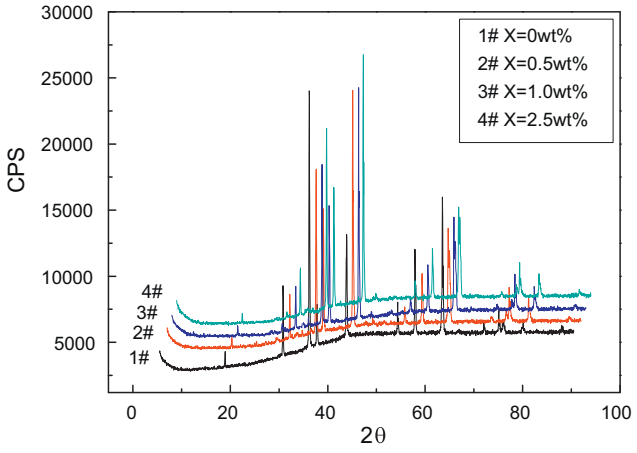

Fig. 2. XRD patterns of samples with different amounts of MnO_2.

indicate that there are three exothermal peaks on the DTA curve at 596.1 °C, 917.7 °C and 1158.4 °C, respectively. It is somewhat different from MnO_2–CeO_2 system [13]. Zhang et al. [14] found that three peaks occurred at 650 °C, 1000 °C and 1200 °C, respectively. They attributed the first peak to the reduction of MnO_2 to Mn_2O_3 and the following two peaks to the reduction of Mn_2O_3 into MnO. For our case, it seems that the reduction of MnO_2 follows the same way through three steps, although the decomposition temperature of each step is lower than that in their case, i.e.

$$2MnO_2 \overset{596.1^\circ C}{\longrightarrow} Mn_2O_3 + \frac{1}{2}O_2 \uparrow \quad (1)$$

$$Mn_2O_3 \overset{917.7^\circ C}{\longrightarrow} 2\,xMnO + (1-x)Mn_2O_3 + \frac{1}{2}xO_2 \uparrow \quad (2)$$

$$(1-x)Mn_2O_3 \overset{1158.4^\circ C}{\longrightarrow} 2(1-x)MnO + \frac{1}{2}(1-x)O_2 \uparrow \quad (3)$$

It can be seen that when sintering temperature is higher than 1158.4 °C, Mn element exists in the state of Mn^{2+} and Mn^{3+} (i.e. MnO and Mn_2O_3) in the $NiFe_2O_4$ spinel lattice. This is in good agreement with the results from XRD analysis in Fig. 2.

Nickel ferrite ($NiFe_2O_4$) is a cubic ferromagnetic material which has an inverse spinel structure with Ni^{2+} ions occupying the octahedral B-sites and Fe^{3+} ions occupying both tetrahedral A-sites and octahedral B-sites. For Ni^{2+} ions preferring to occupy the octahedral B-sites, Mn^{2+} ions have the preference to occupy the A-sites, and Mn^{3+} ions have the preference to occupy the B-sites. This has been

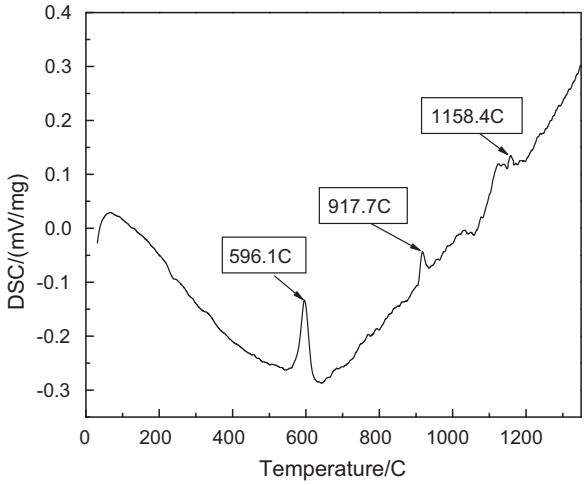

Fig. 3. DSC curve of the sample with 2 wt% MnO_2 additive.

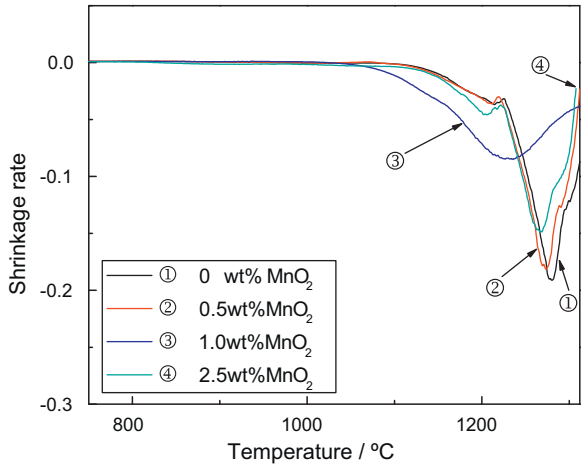

Fig. 4. Shrinkage rate against sintering temperature for ① undoped sample, ② 0.5 wt%, ③ 1 wt% and ④ 2.5 wt% MnO_2-doped ceramic samples sintered at a heating rate of 10 K min^{-1}.

proved in the spinel structure by Bonsdor et al. [14,15]. Fe^{3+} ions in A-sites are mainly substituted by Mn^{2+} ions. Assume all Ni^{2+} ions occupying the octahedral B-sites, the cation distribution formula of nickel ferrite ($NiFe_2O_4$) doped with MnO_2 is represented by:

$$(Mn_{\alpha x}{}^{2+}Fe_{1-\alpha x}{}^{3+})[Ni^{2+}Mn_{(1-\alpha)x}{}^{3+}Fe_{1+(2\alpha-1)x}{}^{3+}]O_4{}^{2+}.$$

3.2. Non-isothermal sintering process

The linear shrinkage ($\Delta L/L_0$) of un-doped and MnO_2-doped ceramic samples sintered at a constant heating rate of 10 K min^{-1} is shown in Fig. 4. The addition of MnO_2 shifts the onset of sintering towards lower temperatures from ~1125 °C for un-doped samples to ~1068 °C for 1 wt% MnO_2-doped ceramic samples.

Fig. 4 shows the linear shrinkage rate ($d(\Delta L/L_0)/dt$) as a function of temperature for different MnO_2 content; there is an obvious decrease in the temperature of maximum shrinkage rate (T_{max}). For example, the temperature of maximum shrinkage rate decreases from 1290 °C for un-doped samples to 1221 °C for 1 wt% MnO_2-doped samples. The difference in the values of T_{max} for both samples is more than 60 °C. When MnO_2 content is up to 2.5 wt%, the T_{max} is lower than that for 1 wt% MnO_2-doped samples. These results suggest that MnO_2 doping can reduce the sintering temperature dramatically. As seen in Fig. 4, the values of T_{max} are sensitive to the doping level in the whole MnO_2 content used. The results obtained from the non-isothermal sintering indicate MnO_2 can promote the densification process and reduce the sintering temperature. Simultaneously, microstructures as shown in Fig. 1 suggest that an appropriate amount of MnO_2 (0–1.0 wt%) can refine the grain and increase the specific surface area of the reaction system. The reaction interface is also enlarged and the sintering activation energy decreased, which is good for accelerating the sintering rate. According to surface theory cited in Ref. [16], the key distribution curve becomes flattened with decreasing grain size to get a higher proportion of weak keys. The excess surface energy for sintering kinetic is enlarged, so the maximum densification rate can be obtained at lower temperatures. It should be noted that a higher doping level (usually >2 cat.%) is ineffective for sintering system. In this work, when more MnO_2 is adopted to the ceramic matrix, only partial MnO_2 entered the lattice of $NiFe_2O_4$, and the excessive MnO_2 accumulated at grain boundaries in ceramic matrix to produce steric hindrance and increase the mass transferring distance, which brought an inhibition of densification for the ceramic matrix.

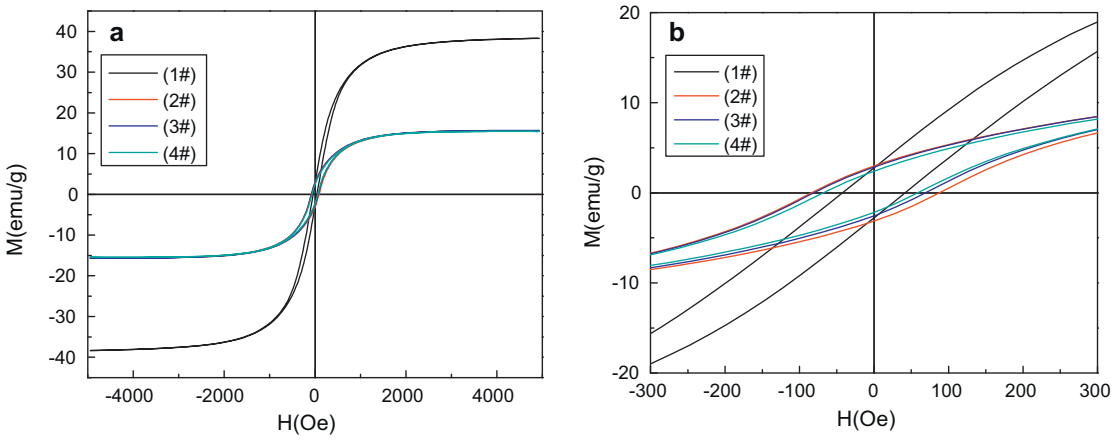

Fig. 5. (a) Magnetic hysteresis loops for ceramic samples doped with different amounts of MnO_2. (b) A part of magnetic hysteresis loops from (a).

Table 1
Magnetic data of MnO_2-doped $NiFe_2O_4$ samples.

	1#	2#	3#	4#
M_s (emu/g)	38.337	15.625	15.673	15.455
M_r (emu/g)	2.776	2.972	2.796	2.399
M_r/M_s	0.0724	0.190	0.178	0.155
H_c (Oe)	32.346	47.696	48.316	39.381

It is verified 1 wt% MnO_2 has better effect on sintering process under the same sintering condition.

3.3. Magnetic properties

The magnetization measurements of each sample were carried out at 300 K using the high field hysteresis loop technique [17]. It is needed to say the samples for magnetization measurements were heated to 1200 °C with a heating rate of 10 K min^{-1}, then sintered for 6 h and cooled down to room temperature. Fig. 5 gives the curve of magnetization versus applied field for ceramic samples with different amounts of MnO_2 (#1 0 wt%; #2 0.5 wt%; #3 1.0 wt%; #4 2.5 wt%). The value of coercivity H_c obtained from the demagnetization curves, saturation magnetization M_s obtained from hysteresis loop and the remnant ratio $R = M_r/M_s$ for ceramic samples are given in Table 1.

With substitution of Mn ions, the saturation magnetization (M_s) decreases. Since MnO_2 decomposed to Mn_2O_3 and MnO during the sintering process, Mn ions entered the $NiFe_2O_4$ spinel lattice in the form of Mn^{3+} and Mn^{2+}. And Mn^{2+} ions have the preference to occupy the A-sites, and Mn^{3+} ions have the preference to occupy the B-sites.

The introduction of Mn^{2+} and Mn^{3+} in place of iron ions into tetrahedral sites and octahedral sites respectively, and presence of nickel ions at octahedral sites dilute both the A and B sublattices simultaneously. According to the radii of the ions listed in Table 2, the incorporation of Mn^{2+} into the A sublattice leads to increase in magnetic moment of A sublattice. Comparing to the decrease in A sublattice, the change caused by Mn^{3+} into the B sublattice can be neglected, because the radii of Mn^{3+} is close to that of Fe^{3+}. So the total magnetic moment decreases. The remnant ratio M_r/M_s is a characteristic parameter of the material. High remnant ratio is an indication of the ease with which the direction of magnetization reorients to nearest easy axis magnetization direction after the magnetic field is removed. The lower value of remnant ratio is indication of isotropic nature of material. It is observed from Table 2 that the values of remnant ratio in the present case are in the range of 0.0724–0.190. It shows increasing trend with Mn ions substitution. It is clearly observed from Table 1 that the coercivity (H_c) increases as Mn ions content increases from the whole aspect. The saturation magnetization is related to H_c through Brown's relation [18], $H_c = 2K_1/\mu_0 M_s$. According to this relation H_c inversely proportional to M_s, this is consistent with our experimental results. The coercivity (H_c) increases rapidly with MnO_2 content up to 1.0 wt%, but above 1.0 wt%, a small change in value has been observed. It may be attributed to the excessive MnO_2 introduction into the matrix, which was favorable for grain coarsening. So the increase in the coercivity value with increasing MnO_2 content is attributed to the increase in the crystallite sizes, as seen in Fig. 1d. It is observed that the values of coercivity for all composition are quite low (H_c < 75 Oe). This indicates that the studied samples retain soft ferrite nature with Mn substitution.

Table 2
All the radii of the ions in the sintered samples.

Element	Mn^{2+}	Mn^{3+}	Mn^{4+}	Fe^{3+}	Ni^{2+}	O^{2-}
Ionic radii (nm)	0.091	0.066	0.052	0.064	0.068	0.14

4. Conclusions

MnO_2-doped nickel ferrites have been synthesized through a standard ceramic technique. X-ray diffraction of the prepared samples shows single phase cubic spinel structure. The decomposition of MnO_2 into Mn_2O_3 and MnO during sintering process is confirmed by differential scanning calorimetry (DSC). The lattice parameter is affected by the content of MnO_2 introduction; the value of lattice parameter for un-doped and 1 wt% MnO_2 doped samples is 8.31 Å and 8.34 Å respectively. Introduction of MnO_2 (i.e. 1.0 wt%) into the ceramic matrix is beneficial to promote sintering process. And MnO_2 doping can reduce the sintering temperature dramatically; the temperature of maximum shrinkage rate decreases from 1290 °C for un-doped samples to 1221 °C for 1 wt% MnO_2-doped samples. The hysteresis loop study shows a decrease in the saturation magnetization (M_s) with increasing MnO_2 content due to the decomposition of Mn^{4+} into Mn^{3+} and Mn^{2+}. And incorporation of Mn^{3+} and Mn^{2+} into the B sublattice and A sublattice respectively leads to the decrease in the total magnetic moment. The residual magnetization ratio (M_r/M_s) and coercivity (H_c) increase in the range of MnO_2 concentration from the whole aspect.

Acknowledgements

The authors gratefully acknowledge the financial support from the State Key Program of National Natural Science of China

(Nos. 50834001 and 50971038) and National High Technology Research and Development Program of China (863 Program) (No. 2009AA03Z502).The authors also thank Professor Gaowu Qin, School of Materials and Metallurgy for utilizing the research facilities available in VSM.

References

[1] S.E. Shirsath, B.G. Toksha, K.M. Jadhav, Mater. Chem. Phys. 117 (2009) 163–168.
[2] A.C.F.M. Costa, V.J. Silva, D.R. Cornejo, M.R. Morelli, R.H.G.A. Kiminami, L. Gama, J. Magn. Magn. Mater. 320 (2008) e370–e372.
[3] Y.M. Al Angari, J. Magn. Magn. Mater. 323 (2011) 1835–1839.
[4] A. Goldman, Modern Ferrite Technology, Marcel Dekker, Inc., New York, 1993.
[5] M.A. Ahmed, S.I. El-Dek, I.M. El-Kashef, N. Helmy, Solid State Sci. (2010) 1–4.
[6] E. Olsen, J. Thonstad, J. Appl. Electrochem. 29 (1999) 293–299.
[7] D.R. Sadoway, JOM 53 (5) (2001) 34–35.
[8] J.L. Berchmans, R.K. Selvan, C.O. Augustin, Mater. Lett. 58 (2004) 1928–1933.
[9] D.R. Patil, B.K. Chougule, Mater. Chem. Phys. 117 (2009) 35–40.
[10] O.M. Hemeda, M.Z. Said, M.M. Barakat, J. Magn. Magn. Mater. 224 (2001) 132–142.
[11] M.A. Gabal, Y.M. Al Angari, Mater. Chem. Phys. 115 (2009) 578–584.
[12] D.W. Ready, J. Am. Ceram. Soc. 49 (1966) 366.
[13] T.S. Zhang, P. Hing, H.T. Huang, J. Kilner, Mater. Sci. Eng. B 83 (2001) 235–241.
[14] X. Zhang, Y.P. Duan, H.T. Guan, S.H. Liu, B. Wen, J. Magn. Magn. Mater. 311 (2007) 507–511.
[15] G. Bonsdorf, M.A. Denecke, K. Schäfer, S. Christen, H. Langbein, W. Gunßer, Solid State Ionics 101 (1997) 351–357.
[16] P.W. May, J.A. Smith, Y.A. Mankelevich, Diam. Relat. Mater. 15 (2) (2006) 345–352.
[17] S.S. Jadhav, S.E. Shirsath, B.G. Toksha, S.J. Shukla, K.M. Jadhav, J. Chem. Phys. 21 (2008) 1.
[18] J.M.D. Coey, Rare Earth Permanent Magnetism, John Wiley and Sons, New York, 1996.